

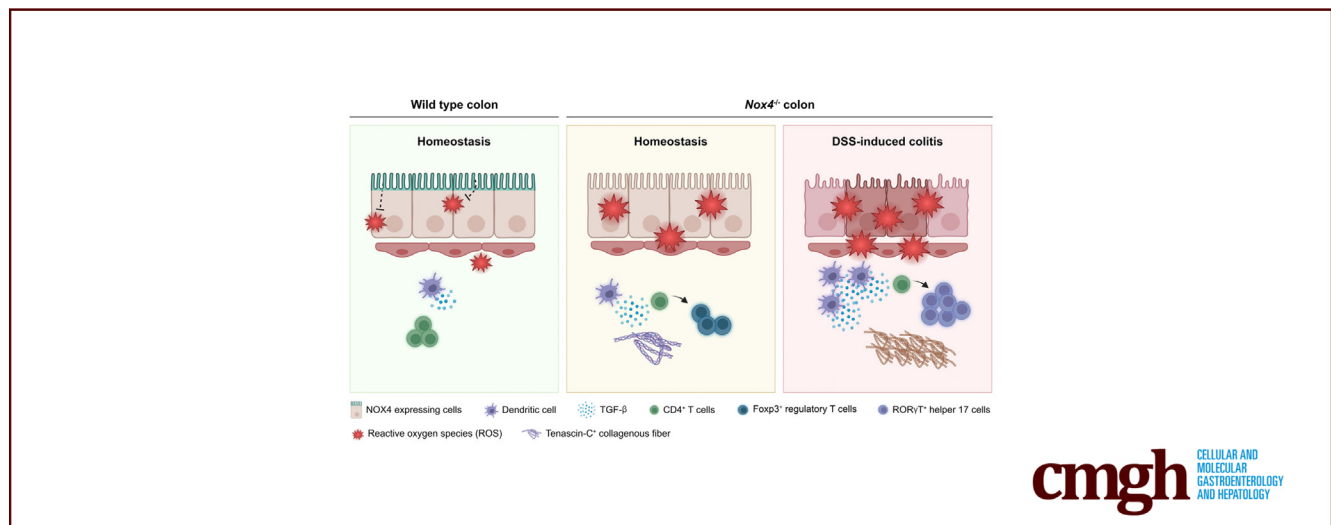
ORIGINAL RESEARCH

Role of Nox4 in Mitigating Inflammation and Fibrosis in Dextran Sulfate Sodium–Induced Colitis



Yura Lee,¹ Sung-Hee Kim,¹ Haengdueng Jeong,¹ Kwang H. Kim,¹ Donghun Jeon,¹ Yejin Cho,¹ Daekee Lee,² and Ki Taek Nam¹

¹Severance Biomedical Science Institute, Brain Korea 21 PLUS Project for Medical Science, Yonsei University College of Medicine, Seoul, Korea; and ²Department of Life Science, Ewha Womans University, Seoul, Korea



BACKGROUND & AIMS: Fibrosis development in ulcerative colitis is associated directly with the severity of mucosal inflammation, which increases the risk of colorectal cancer. The transforming growth factor- β (TGF- β) signaling pathway is an important source of tissue fibrogenesis, which is stimulated directly by reactive oxygen species produced from nicotinamide adenine dinucleotide phosphate oxidases (NOX). Among members of the NOX family, NOX4 expression is up-regulated in patients with fibrostenotic Crohn's disease (CD) and in dextran sulfate sodium (DSS)-induced murine colitis. The aim of this study was to determine whether NOX4 plays a role in fibrogenesis during inflammation in the colon using a mouse model.

METHODS: Acute and recovery models of colonic inflammation were performed by DSS administration to newly generated *Nox4*^{-/-} mice. Pathologic analysis of colon tissues was performed, including detection of immune cells, proliferation, and fibrotic and inflammatory markers. RNA sequencing was performed to detect differentially expressed genes between *Nox4*^{-/-} and wild-type mice in both the untreated and DSS-treated conditions, followed by functional enrichment analysis to explore the molecular mechanisms contributing to

pathologic differences during DSS-induced colitis and after recovery.

RESULTS: *Nox4*^{-/-} mice showed increased endogenous TGF- β signaling in the colon, increased reactive oxygen species levels, intensive inflammation, and an increased fibrotic region after DSS treatment compared with wild-type mice. Bulk RNA sequencing confirmed involvement of canonical TGF- β signaling in fibrogenesis of the DSS-induced colitis model. Up-regulation of TGF- β signaling affects collagen activation and T-cell lineage commitment, increasing the susceptibility for inflammation.

CONCLUSIONS: *Nox4* protects against injury and plays a crucial role in fibrogenesis in DSS-induced colitis through canonical TGF- β signaling regulation, highlighting a new treatment target. (*Cell Mol Gastroenterol Hepatol* 2023;16:411–429; <https://doi.org/10.1016/j.jcmgh.2023.05.002>)

Keywords: Fibrostenotic CD; T-Cell Lineage Commitment; RNA-Sequencing; Oxidative Stress.

Ulcerative colitis (UC) is a common form of inflammatory bowel disease (IBD) resulting from long-term inflammatory damage and ulceration of the colonic mucosa. Continuous inflammation by commensal bacteria affects the intestinal epithelial barrier and is a major contributor to UC pathogenesis.¹ Current therapies are ineffective for most patients with UC, and are associated with adverse events such as tissue function abnormalities, fibrostenosis, and malignant transformation.² UC-associated carcinogenesis derives mainly from the inflammation-mediated production of excessive reactive oxygen species (ROS) in damaged tissues, and the consequent impairment of redox balance leads to oxidative stress after molecular damage (lipid, DNA, protein), along with genetic variation in the transforming colon cells, eventually causing colorectal cancer. Given the poor prognosis of UC-associated colorectal cancer, there is an urgent need to identify novel therapeutic targets.

Members of the nicotinamide adenine dinucleotide phosphate oxidase (NOX) family are mainly responsible for ROS production in the gastrointestinal tract, which play roles in pathogen clearance,³ maintenance of barrier function,⁴ and mucosal repair after injury.⁵ Specifically, *NOX1* and dual oxidase (DUOX) 2 are expressed abundantly in the intestinal epithelium as the primary sources of ROS in the intestinal mucosa, and their mutation has been linked to the risk of adult IBD. *NOX1* contributes to intestinal homeostasis by regulating mucus cell differentiation,⁶ migration, microbial defense, and mediation of mucus repair after injury.^{7,8} *DUOX2* is activated by pathogen-derived uracil⁹ to produce *DUOX*-dependent ROS and governs gut microbe clearance¹⁰ caused by enteric infection.

Several recent studies have elucidated the roles of *NOX4* in regulating inflammation-mediated pathophysiology in the colon. *NOX4* produces H_2O_2 , and is expressed predominately in vascular smooth muscle cells, endothelial cells, and fibroblasts in most tissues. *NOX4* expression is up-regulated in drug-resistant patients with UC¹¹ and fibrostenotic Crohn's disease (CD),¹² and in dextran sulfate sodium (DSS)-induced murine colitis models.^{13,14} *Nox4* transcripts are detected at low levels in the normal colon,¹⁵ but increase to protect against DSS-induced^{16,17} and bacterial-induced¹⁷ murine colitis. The related mechanism likely involves *NOX4*-driven ROS production, which induces the phosphorylation of p65 to activate nuclear factor- κ B signaling and the M1 phenotype of intestinal macrophages, leading to mucosal barrier injury to promote colitis progression.¹⁶ Although *NOX4* has rarely been associated with the development of fibrogenic features in mouse colitis models,¹⁷ the main pathologic mechanism contributing to fibrotic disease in the lung,¹⁸ liver,¹⁹ kidney,²⁰ and heart²¹ is attributed to ROS-induced canonical transforming growth factor- β (TGF- β) signaling, and redox signaling driven by *NOX4* is closely related to canonical TGF- β signaling to cause a TGF- β -induced profibrotic response.²² However, the detailed molecular mechanism underlying fibrosis development in UC remains to be elucidated.

Based on this background, we hypothesized that *NOX4* contributes to intestinal fibrotic injury in UC and is required for TGF- β signaling inducing fibrosis development. To test this

hypothesis, we established *NOX4*-deficient mice (*Nox4*^{-/-}) with DSS-induced colitis. RNA-sequencing (RNA-seq) analysis was performed to explore the effects of *Nox4* on the response to intestinal damage. This study highlights the role of *Nox4* in inducing inflammation in the colon, suggesting that exploiting the redox signal can be a double-edged sword and should be considered carefully for the effective treatment of UC.

Results


Nox4 Protects Against DSS-Induced Experimental Colitis

To study the role of *Nox4* in fibrogenesis in DSS-induced colitis in mice, first we confirmed *NOX4* expression in the tissues.

We performed immunohistochemistry in the normal and DSS-treated inflamed colon sections. In the normal colon, *NOX4* was detected at the top of the crypt, and *NOX4* proteins increased significantly in the injured mucosa (not only at the top, but also at the bottom, of the crypt) after 2.5% DSS-induced colitis (Figure 1C). Loss of *Nox4* increased the production of ROS in the control (Figure 1E) and DSS-induced colitis model (Figure 1F), suggesting that *Nox4* increase might be associated with disease progression.

After inducing the inflammatory phase with DSS treatment (W/DSS) (Figure 2A), *Nox4*^{-/-} mice showed severe inflammation with rapid body weight loss of approximately 20%–30% (Figure 2B) and decreased survival (Figure 2C) compared with that of wild-type (WT) mice. Macroscopic and histologic observations showed that W/DSS *Nox4*^{-/-} mice had shorter colon lengths (Figure 2D) and more severe inflammatory regions in the distal colon, including infiltration of inflammatory cells into the lamina propria, transmural inflammation, and loss of the crypt and surface epithelium (Figure 2E and F). W/DSS *Nox4*^{-/-} mice showed higher Disease Activity Index (DAI) scores from 1 to 14 days than the W/DSS WT group (Figure 2G). The W/DSS *Nox4*^{-/-} colon showed 1.5-fold higher H_2O_2 /ROS production than the W/DSS WT colon (Figure 1G). These results could suggest that *Nox4* is involved in the regulation of ROS in the colonic issue, which contributes to the inflammatory response.

Abbreviations used in this paper: CIBERSORT, Cell-type Identification by Estimating Relative Subsets of RNA Transcripts; DAI, Disease Activity Index; DEG, differentially expressed gene; DSS, dextran sulfate sodium; ELISA, enzyme-linked immunosorbent assay; FACS, fluorescence-activated cell sorter; Foxp3, Forkhead box P3; GO, Gene Ontology; IBD, inflammatory bowel disease; IL, interleukin; KEGG, Kyoto Encyclopedia of Genes and Genomes; mRNA, messenger RNA; NOX, nicotinamide adenine dinucleotide phosphate oxidase; PCR, polymerase chain reaction; pSmad2/3, Phosphorylated Smad2/3; RNA-seq, RNA sequencing; ROR γ T, Retinoid orphan receptor gamma t; ROS, reactive oxygen species; Smad, Small Mothers Against Decapentaplegic; TGF- β , transforming growth factor- β ; TGF β R, Transforming growth factor- β receptor; Th17, T helper 17 cells; Treg, regulatory T cell; WT, wild type; W/DSS, with dextran sulfate sodium treatment; UC, ulcerative colitis.

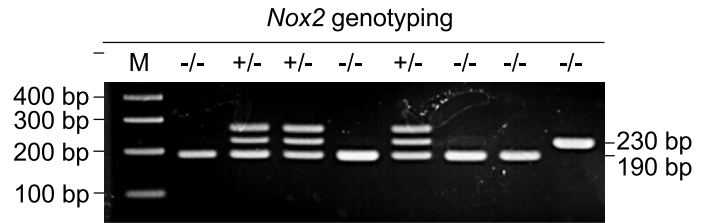
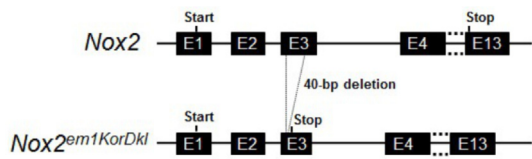
 Most current article

© 2023 The Authors. Published by Elsevier Inc. on behalf of the AGA Institute. This is an open access article under the CC BY-NC-ND license (<http://creativecommons.org/licenses/by-nc-nd/4.0/>).

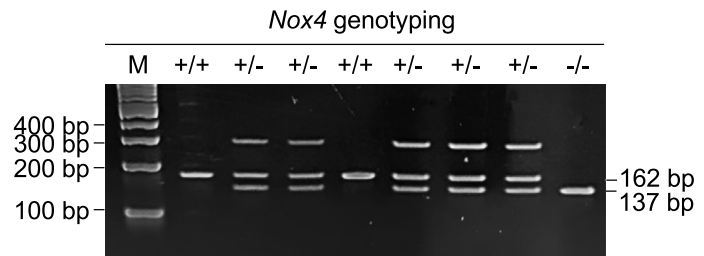
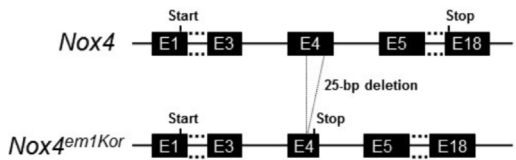
2352-345X

<https://doi.org/10.1016/j.jcmgh.2023.05.002>

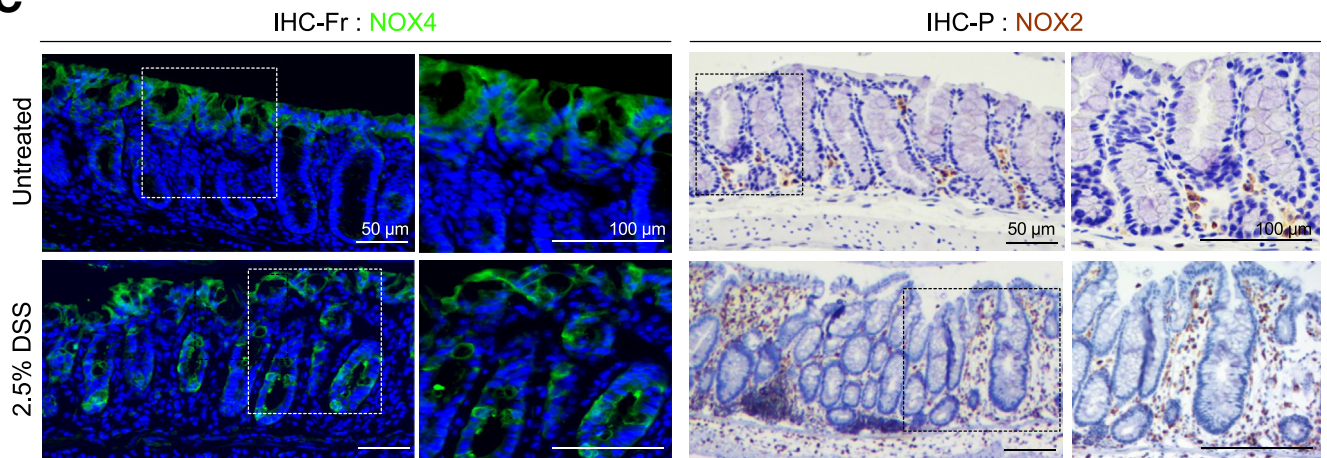
A



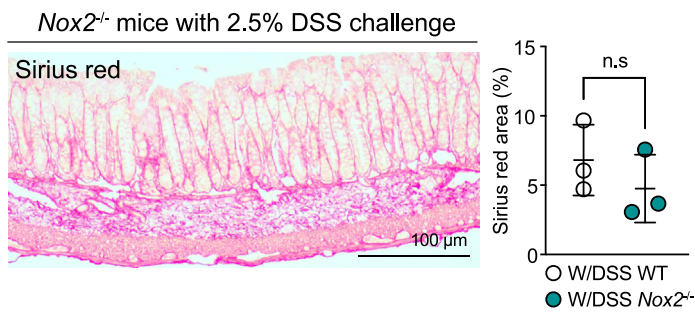
B



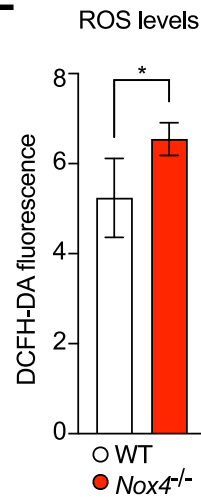
C



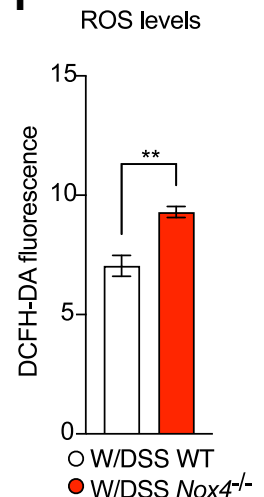
D



E



F



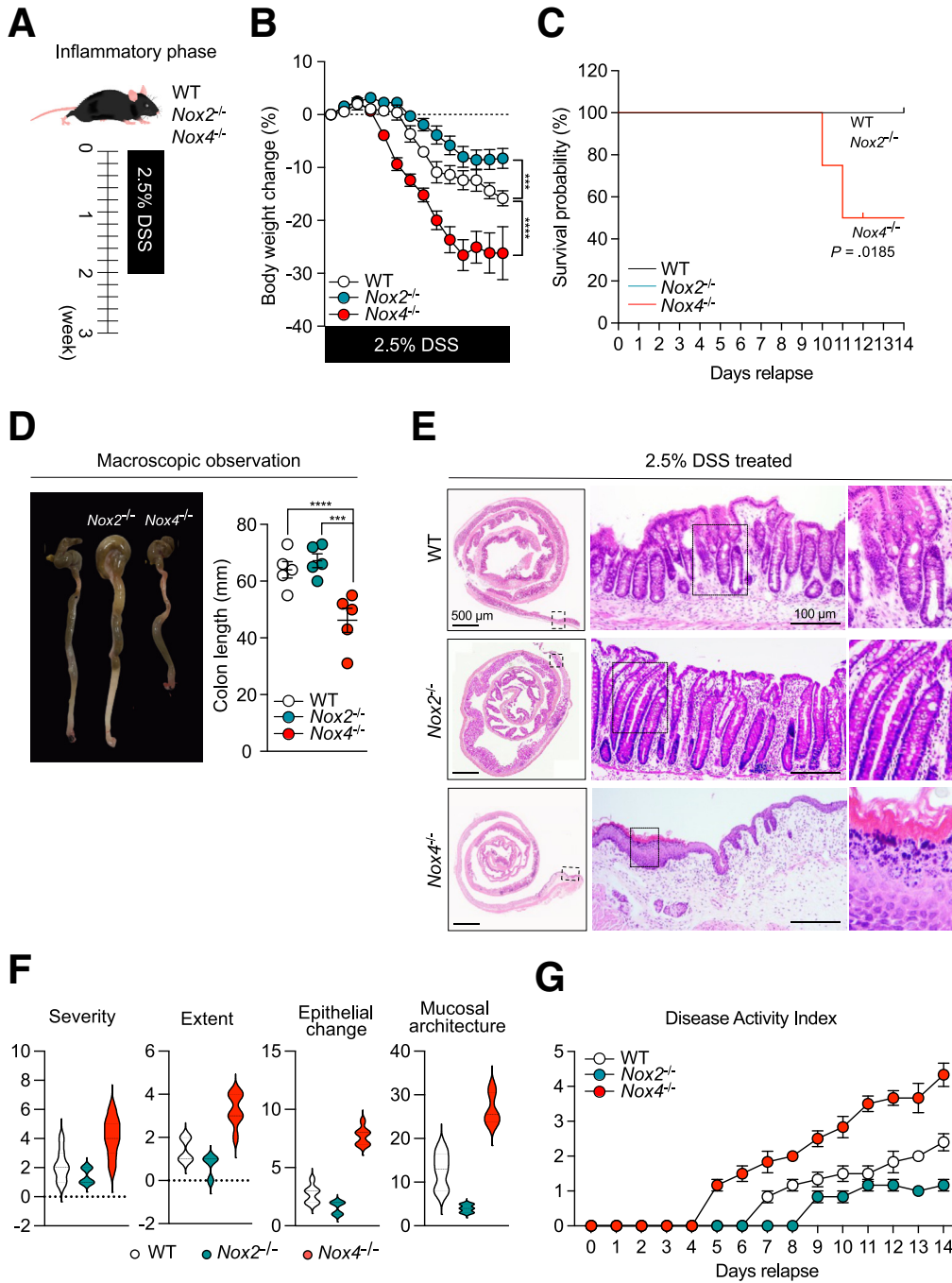


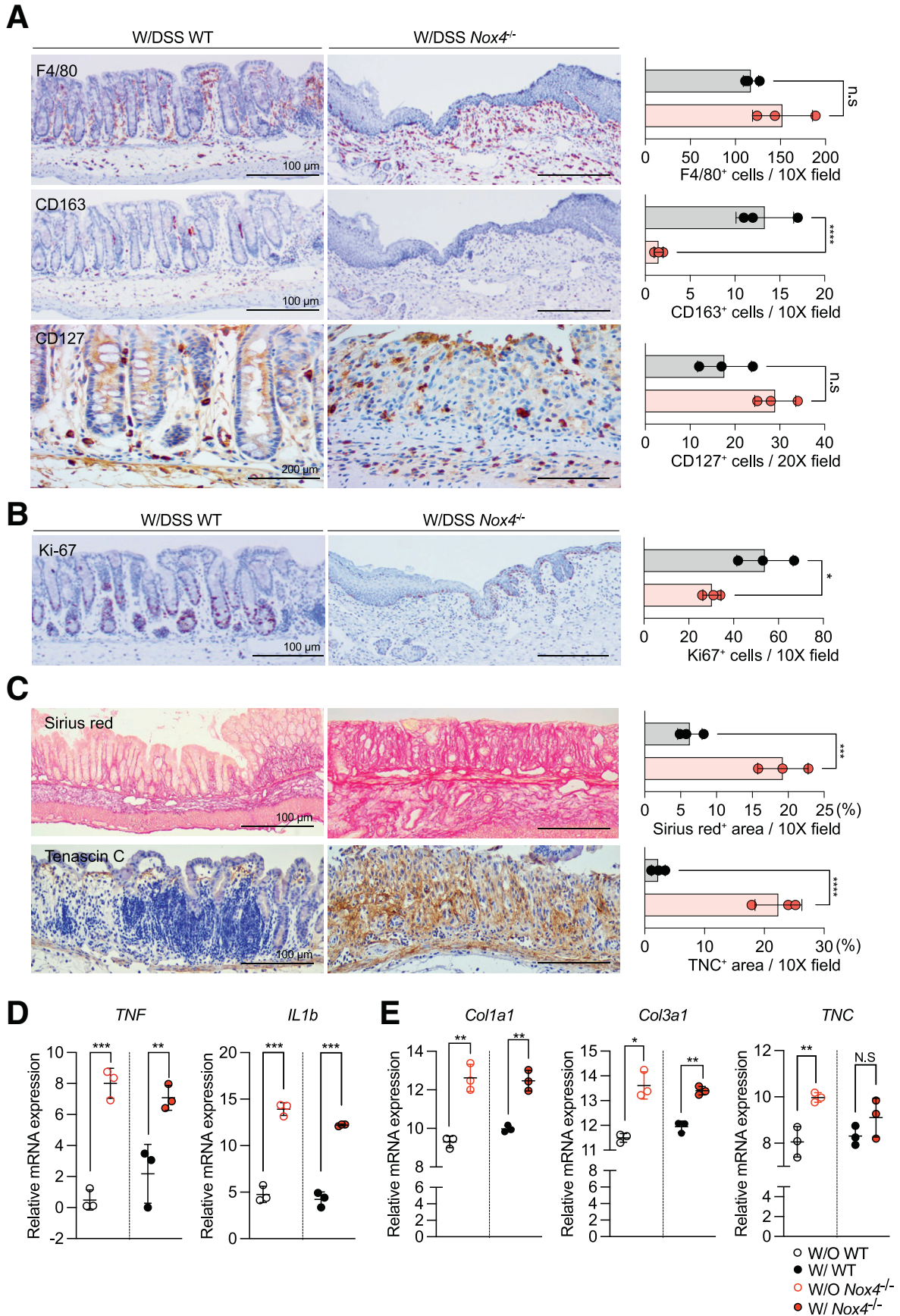
Figure 2. *Nox4* protects against DSS-induced experimental colitis.

(A) Experimental scheme for the DSS-induced murine colitis model. (B) Body weight loss for WT and *Nox2*^{-/-} mice with DSS-induced colitis was measured daily (n = 6). (C) Survival probability of WT or *Nox4*^{-/-} mice with DSS-induced colitis was assessed until day 14 (n = 6). (D) Macroscopic observation of the colons from WT and *Nox4*^{-/-} mice with DSS-induced colitis killed on day 14. Colon lengths were assessed after the mice were killed. (E) Representative H&E staining images of colon tissues from DSS-induced colitis WT and *Nox4*^{-/-} mice. (F) Colitis scoring for pathologic assessment in DSS-induced colitis WT and *Nox4*^{-/-} mice: severity, inflammation severity (0–3); extent, inflammation extent (0, none; 1, mucosa; 2, submucosa; and 3, transmural), and epithelial change. (G) Disease activity index comprising assessment of body weight loss, stool consistency, and rectal bleeding measured daily. Data are expressed as means ± SD. ****P* < .005, and *****P* < .001 compared with WT.

Nox2 was expressed mainly in the immune cells²³ (Figure 1C). In line with the results of a previous study,²⁴ W/DSS *Nox2*^{-/-} mice did not develop severe colitis, and the

body weight change decreased less than that found for W/DSS WT mice (Figure 2B). Moreover, W/DSS *Nox2*^{-/-} mice showed high survival rates (Figure 2C), and there was no

Figure 1. (See previous page). Generation of *Nox4*^{-/-} mice. Schematic representation of (A) *Nox2* and (B) *Nox4* deletion using CRISPR/Cas9 technology. The resulting heterozygous and homozygous mice were determined by genotyping PCR using a specific *Nox2* or *Nox4* deletion site. (C) Immunofluorescence images for NOX4 on the untreated colon and 2.5% DSS-treated colon frozen sections (immunohistochemistry [IHC]-Fr) (left). IHC for NOX2 on the untreated colon and 2.5% DSS-treated colon paraffin-embedded sections (IHC-P) (right). (D) Sirius-red staining showing the fibrotic area in red. The graph represents the measurement of the fibrotic area using ImageJ (National Institutes of Health). Intracellular levels of ROS in the (E) untreated and (F) DSS-treated groups assessed using DCFH-DA staining followed by flow cytometry. Data are expressed as means ± SD. **P* < .5 and ***P* < .01 compared with WT. bp, base pair; DCFH-DA, dichloro-dihydro-fluorescein diacetate.



change in the colon length from that of WT mice (Figure 2D). Histologic examination of the DSS-treated W/DSS *Nox2*^{-/-} colon revealed elongated crypts, immune cell infiltration, and goblet cell loss (Figure 1D), indicating an injured colon; however, the damage score was decreased significantly compared with the W/DSS WT and W/DSS *Nox4*^{-/-} mice (Figure 2F and G). In line with these results, W/DSS *Nox2*^{-/-} mice did not develop fibrotic regions in the colon after DSS administration (Figure 1D). Thus, *Nox2* deficiency results in mild inflammation in DSS-induced colitis, whereas W/DSS *Nox4*^{-/-} mice showed severe colonic damage upon DSS treatment; accordingly, we further investigated the characteristics of inflammation in *Nox4*^{-/-} mice.

Nox4 Deficiency Increases Intestinal Fibrosis After DSS-Induced Colitis

Immunohistochemistry showed that F4/80⁺ M1 macrophages were increased (Figure 3A, top), whereas CD163⁺ M2 macrophages were decreased significantly (Figure 3B, middle) in the *Nox4*^{-/-} colon tissue compared with those of the WT colon. CD127⁺ lymphoid cells also were increased in DSS-induced colitis *Nox4*^{-/-} mice (Figure 3A, bottom). Ki-67 immunostaining showed an increase in cell proliferation in the DSS-induced colitis WT colon compared with that of the DSS-induced colitis *Nox4*^{-/-} mice (Figure 3B). This result indicated that *Nox4*^{-/-} mice did not show a typical repair response to colitis-induced damage. Sirius red staining showed increased intestinal fibrosis (Figure 3C, top), which corresponded with increased expression of typical fibrosis markers such as *Col1a1* and *Col3a1* (Figure 3E) detected by reverse-transcription quantitative polymerase chain reaction (PCR). The specific diagnostic marker of collagenous colitis, Tenascin-C, was increased remarkably in the colitis-induced *Nox4*^{-/-} colon at both the protein (Figure 3C, bottom) and messenger RNA (mRNA) (Figure 3E) levels compared with those in colitis-induced WT mice. Furthermore, the mRNA levels of the inflammatory cytokines tumor necrosis factor (*Tnf*) and interleukin 1 β (*Il1 β*) were increased significantly in colitis-induced *Nox4*^{-/-} mice (Figure 3D) compared with those of WT mice at the same time points. Moreover, in the untreated condition (without DSS), *Nox4*^{-/-} mice also showed an increase in the proteins of the F4/80⁺ macrophage and Ki-67⁺ proliferating cells (Figure 4A). Further, the mRNA levels of fibrosis-related markers and proinflammatory cytokines such as *Tnf* and *Il1 β* were significantly increased in colitis induced *Nox4*^{-/-} mice compared with those in WT mice at the same

points. (Figure 3D and E). In addition, the colons of untreated *Nox4*^{-/-} mice also had a greater fibrotic area, as detected by Tenascin-c immunostaining, compared with that of the WT colon (Figure 4B). These results suggest that the more severe inflammatory response to DSS induction in *Nox4*^{-/-} mice is related to the activation of intestinal inflammation and fibrosis resulting from *Nox4* deficiency.

Differential Gene Expression Under *Nox4* Deficiency in the Distal Colon Tissue

Bulk RNA-seq analysis was performed to identify the underlying mechanism contributing to the more severe inflammation and fibrosis in *Nox4*^{-/-} mice (Figure 5A). A total of 5124 differentially expressed genes (DEGs) were identified among the 4 comparisons (W/O *Nox4*^{-/-} vs W/O WT; W/*Nox4*^{-/-} vs W/WT; W/WT vs W/O WT; and W/*Nox4*^{-/-} vs W/O *Nox4*^{-/-}). Comparing the treated and untreated groups, 42 genes were co-up-regulated, and 2 genes were co-down-regulated (Figure 5B). The 42 co-regulated genes included T-cell-related genes (*CD3e* and *Tnfrsf9*),²⁵ fibroblast activators (*Itg2a*²⁶ and *Vegf*),²⁷ inflammasome sensor (*Nlrp3*), and TGF- β target genes (*Ano5* and *Muc11*) with higher expression levels in *Nox4*^{-/-} than in WT mice. For the untreated comparison, genes identified as colorectal cancer biomarkers, such as *Tnfrsf4*, *Fabp47*, *CD79b*, and *Ptgs2*,²⁸ were down-regulated in *Nox4*^{-/-} mice compared with those in WT mice (Figure 5C). These findings suggest that *Nox4* deficiency suppresses TGF- β signaling, which acts as a tumor-suppressor factor in normal cells.²⁹

Functional enrichment analysis of the DEGs, including Gene Ontology (GO) and Kyoto Encyclopedia of Genes and Genomes (KEGG) enrichment, was performed using Database for Annotation, Visualization, and Integrated Discovery tools to assess the biological functions increased in *Nox4*^{-/-} compared with WT mice. The GO analysis indicated that most of the DEGs in *Nox4*^{-/-} mice were enriched in collagen-associated responses, TGF- β stimulus, and cellular repair processes (Figure 5D). In addition, KEGG analysis showed high expression of in *Nox4*^{-/-} DEGs related to the type 2 immune response, collagen process, and inflammatory response (immune system process, response to lipopolysaccharide, and redox process) (Figure 5E). Further investigation using Cell-type Identification by Estimating Relative Subsets of RNA Transcripts (CIBERSORT) with 11 immune signature gene sets showed that the *Nox4*^{-/-} colon had predominantly increased regulatory T cells (Tregs) and decreased plasma cells compared with the WT colon (Figure 5F and G). Flow cytometry of the colon tissue

Figure 3. (See previous page). *Nox4* is involved in intestinal fibrosis and immune-mediated tissue regeneration. (A) Immunohistochemistry with antibodies against F4/80 (top) indicating M1 macrophages, CD164 (middle) indicating M2 macrophages, and CD127 (bottom) indicating lymphoid cells on DSS-treated WT and *Nox4*^{-/-} mouse colon sections. (B) Immunohistochemistry with antibody against Ki-67 indicating proliferating cells. (C) Sirius red staining showing the fibrotic area in red (top). Immunolabeling with antibodies against Tenascin-C indicates fibrosis in the colon tissue (bottom). Each positive staining area was measured by ImageJ and shown as a bar graph. Grey, WT group (N = 3); red, *Nox4*^{-/-} group (N = 3). (D) Reverse-transcription quantitative PCR results of proinflammatory-related genes *TNF*, and *IL1b*. (E) Reverse-transcription quantitative PCR results of fibrosis-related genes *Col1a1*, *Col3a1*, and *TNC*. Data are expressed as means \pm SD. **P* < .05, ***P* < .01, ****P* < .005, and *****P* < .001 compared with WT. Ki-67, marker of proliferation Ki(Kiel)-67.

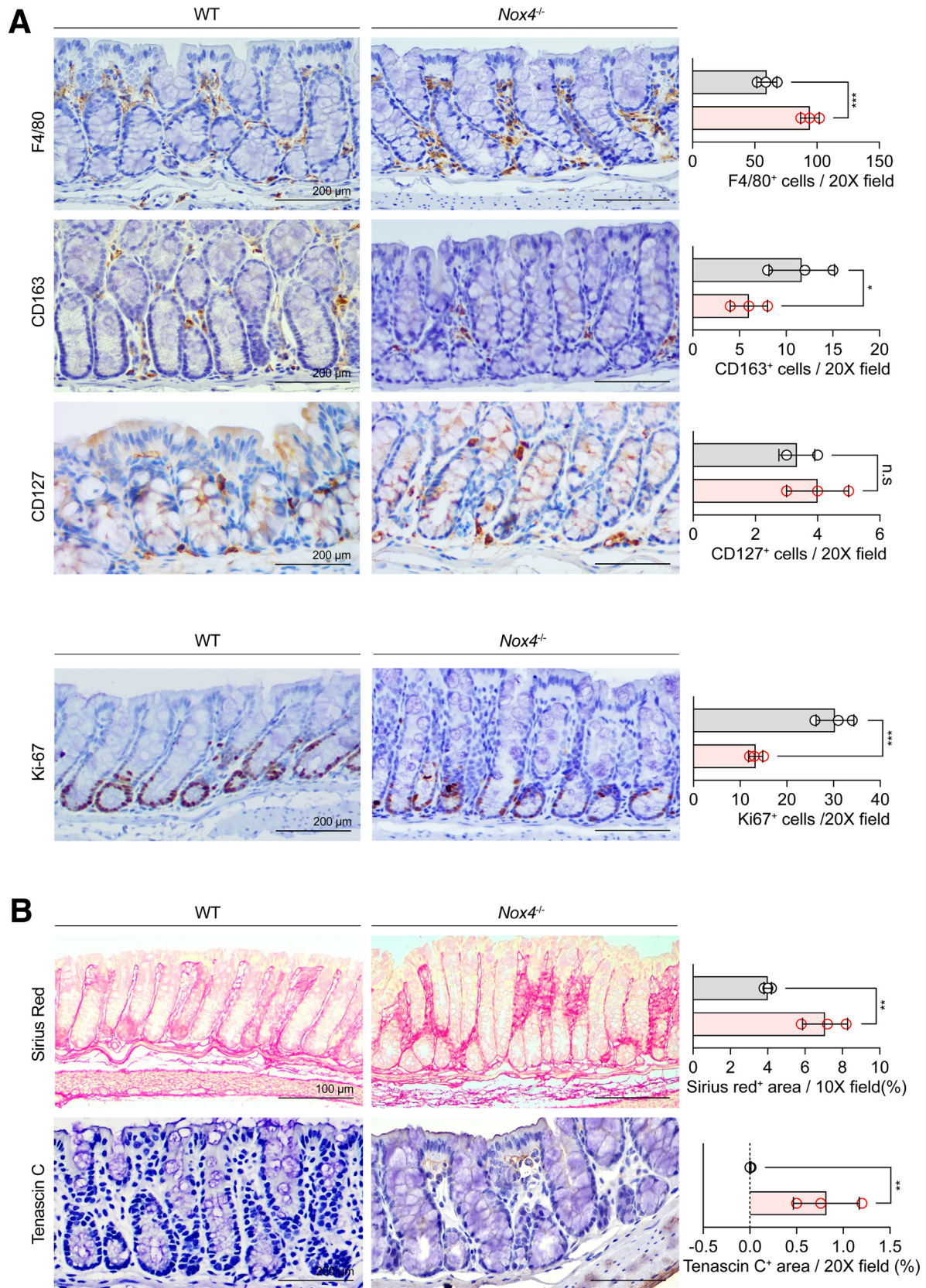
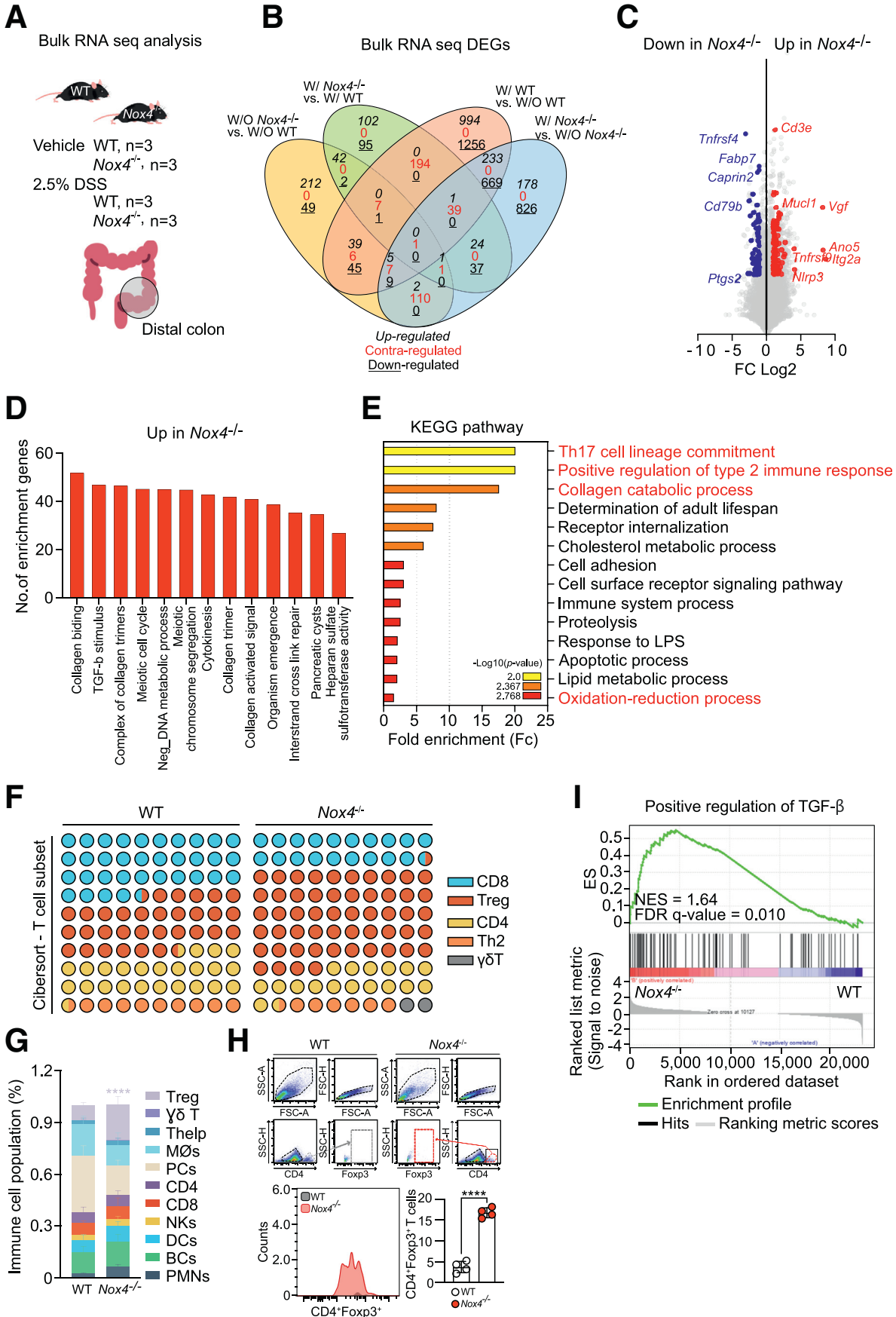


Figure 4. Immune cell infiltration in the WT and Nox4^{-/-} mouse colon. (A) Immunohistochemistry with antibodies against F4/80 indicating M1 macrophages, CD164 indicating M2 macrophages, CD127 indicating lymphoid cells, and Ki-67 (bottom) indicating proliferating cells. (B) Sirius-red staining showing the fibrotic area in red (top). Immunolabeling with antibodies against Tenascin-C indicating fibrosis in the colon tissue (bottom). Each positive staining area and cell was measured by ImageJ and shown as a bar graph. The WT group (N = 3) is colored gray and the Nox4^{-/-} group (N = 3) is colored red. Data are expressed as means ± SD. *P < .05, **P < .01, and ***P < .005 compared with WT. Ki-67, marker of proliferation Ki(Kiel)-67.



confirmed a 4-fold increase in CD4⁺Foxp3⁺ Tregs caused by loss of *Nox4* (Figure 5H).

Nox4 Deficiency Activates the Canonical TGF- β Signaling Pathway

Gene set enrichment analysis confirmed up-regulation of the TGF- β signaling stimulatory gene set in *Nox4*^{-/-} DEGs compared with WT DEGs (Figure 5I). Given recent studies highlighting a role of *Nox4* in regulating the canonical TGF- β signaling pathway in lung fibrosis³⁰ and pancreatic cancer,³¹ we further focused on the role of *Nox4* in canonical TGF- β signaling in the murine colon. Activation of canonical TGF- β signaling involves binding of TGF- β to TGF β R2, which then phosphorylates TGF β R1 to subsequently induce the phosphorylation of Smad2/3 (pSmad2/3) and Smad4, ultimately promoting the translocation of pSmad2/3 and Smad4 to the nucleus (Figure 6A). We observed higher mRNA expression of *Tgfb1* in the *Nox4*^{-/-} colon tissue than in the nontreated WT colon, whereas there were no differences in the mRNA levels of *Tgfb2* and *Tgfb1* between the 2 groups (Figure 6B). An enzyme-linked immunosorbent assay (ELISA) showed that an active form of TGF- β was increased in the *Nox4*^{-/-} colon compared with the WT colon (Figure 6C). Consistently, Western blot showed that TGF- β and TGF β R1 protein levels were increased in the *Nox4*^{-/-} colon tissue lysate compared with those of the WT group (Figure 6D). To validate the TGF β R1-induced phosphorylation of Smad2/3, total Smad2/3, and Smad4, the cytosol-nuclear fraction of each colon tissue lysate was evaluated, showing increased translocation of cytosolic pSmad2/3 and Smad4 to the nucleus of the *Nox4*^{-/-} colon compared with the WT colon (Figure 6E). TGF- β ⁺ cells were expressed in the lamina propria rather than in the epithelium in the *Nox4*^{-/-} colon, along with a significantly higher number of TGF- β ⁺ cells (Figure 6F). Immunofluorescence staining further showed co-expression of CD11c⁺ dendritic cells in TGF- β ⁺ cells in the colon (Figure 6G). Overall, these results strongly suggested that *Nox4* depletion leads to canonical TGF- β activation in the colon, thereby inducing fibrotic gene expression and Treg commitment.

Nox4 Deficiency Exacerbates Experimental Colitis via Inducing the TGF- β Pathway to Promote Intestinal Inflammation

Based on these results, we further analyzed the bulk RNA-seq data of DSS-treated WT and *Nox4*^{-/-} mice to

determine whether the TGF- β signal continuously affects intestinal inflammation during DSS-induced colitis. Principal component analysis showed that the W/DSS *Nox4*^{-/-} transcripts were clearly discriminated from those of W/DSS WT mice (Figure 7A). A total of 427 DEGs ($P < .05$; fold change, >2) were identified between the 2 groups, with 247 up-regulated genes and 179 down-regulated genes in W/DSS *Nox4*^{-/-} mice compared with W/DSS WT mice (Figure 7B). Notably, in the W/DSS *Nox4*^{-/-} mice, the expression levels of TGF- β -related genes such as *Asap3* and *Tgfb1*, which are positive regulators of the TGF- β pathway; inflammation-mediated Th17 cell differentiation genes such as *Plekha4*¹⁴ and *Batf*^{32,33}; and fibrosis-related genes such as *Acta1* and *Myo6*, which promote the synthesis of collagen,³⁴ were increased. However, in the W/DSS WT mice, UC-related genes such as *Chic1*, *Ido1*, and *Reg3g*,^{35,36} and immune infiltrate-related genes such as *Tmco3*,³⁷ *Orai2*,³⁸ and *Saa2*,³⁹ were up-regulated (Figure 7C). Using CIBERSORT, we confirmed that the proportion of Th17 cells was increased significantly in the W/DSS *Nox4*^{-/-} colon compared with that of the W/DSS WT colon (Figure 7D and E).

GO analysis of the W/DSS WT or W/DSS *Nox4*^{-/-} DEGs showed enrichment of up-regulated W/DSS WT DEGs in the cellular component (GO-CC) related to colitis-mediated functions such as innate immune response, biotic stimulus, and cytokine production, and tissue repair programs such as wound healing and defense response (Figure 8A). Similarly, up-regulated W/DSS WT DEGs were enriched in biological processes (GO-BP) of endoplasmic reticulum stress associated with intestinal inflammation, such as innate immune response and cytokine production, and tissue recovery-related processes.⁴⁰ The DEGs were enriched in molecular function GO terms (GO-MF) included in the IBD pathophysiology-related gene set,⁴¹ such as calcium ion binding, peptidase activity, and signal transduction-related functions (Figure 8A). However, the W/DSS *Nox4*^{-/-} DEGs showed a different functional pattern. For GO-CC, the DEGs were enriched in tissue damage gene sets such as apoptosis, inflammation, and damage. Furthermore, the top-enriched gene sets in biological processes were identified as tissue fibrosis-related gene sets,⁴² such as the catalytic complex, cytoskeletal part, and ribonucleoprotein complex. For GO-MF, highly enriched DEGs were verified as UC-associated oncogenic gene sets such as protein binding, protein

Figure 5. (See previous page). Loss of *Nox4* leads to collagen synthesis and Treg lineage commitment. (A) Scheme for bulk RNA-seq analysis of freshly isolated distal colon tissues comparing transcriptomes from the vehicle group in WT ($n = 3$) and *Nox4*^{-/-} ($n = 3$) mice or the 2.5% DSS-treated colitis group in WT ($n = 3$) and *Nox4*^{-/-} ($n = 3$) mice. (B) Venn diagram analysis of the 5124 DEGs comparing the numbers of up-regulated, contraregulated, and down-regulated within each control and experimental group. (C) Volcano plot identifying genes significantly down-regulated (blue) and up-regulated (red) with a more than 2-fold express level difference in *Nox4*^{-/-} compared with WT samples. (D) GO biological process analysis of up-regulated DEGs in *Nox4*^{-/-} mice. (E) KEGG pathway enrichment analysis of *Nox4*^{-/-} DEGs. The top 14 pathways are identified, and the colors indicate statistical significance. (F) T-cell subpopulation evaluated by CIBERSORT based on WT and *Nox4*^{-/-} DEGs. (G) CIBERSORT analysis of WT and *Nox4*^{-/-} colon tissue. The relative proportions of 11 different immune cell types are deconvoluted from the RNA-seq data using CIBERSORT. (H) Flow cytometry analysis of freshly isolated WT or *Nox4*^{-/-} distal colon tissue showing the relative number of live cells gated on CD4⁺Foxp3⁺ T cells (*top*, histogram) and the number of CD4⁺Foxp3⁺ T cells (*bar graph*, *bottom*). (I) Gene set enrichment analysis based on WT or *Nox4*^{-/-} DEGs. Positive regulation of the TGF- β gene set is enriched with genes up-regulated in the *Nox4*^{-/-} mouse colon. BC, B cell; DC, Dendritic cell; FDR, False discovery rate; FSC-A, Forward scatter-area; FSC-H, Forward scatter-height; ES, Enrichment score; LPS, lipopolysaccharide; NES, Normalized enrichment score; NK, Natural killer; PC, Plasma cell; PMN, Polymorphonuclear leukocyte; SSC-A, Side scatter-area; SSC-H, Side scatter-height.

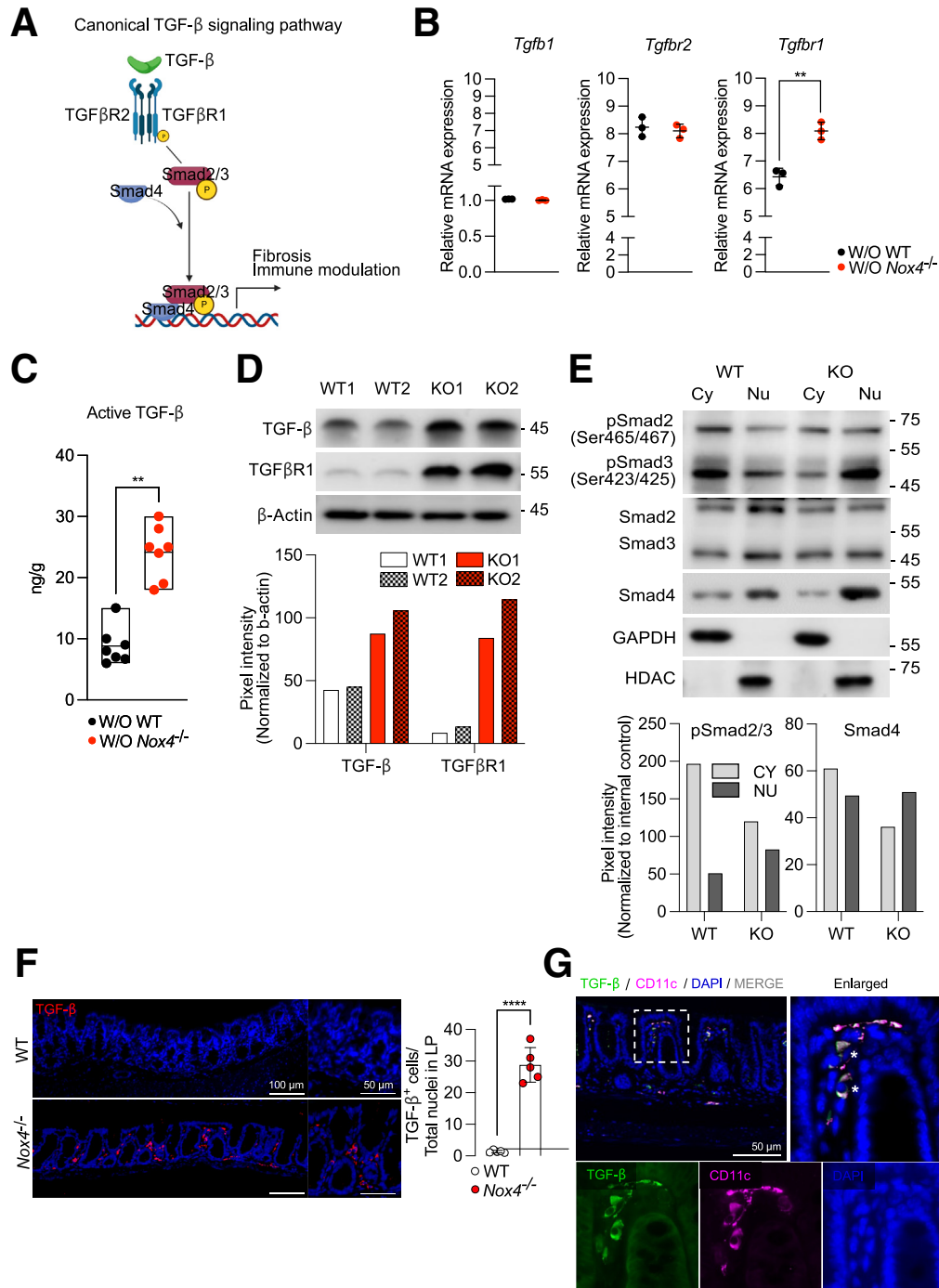
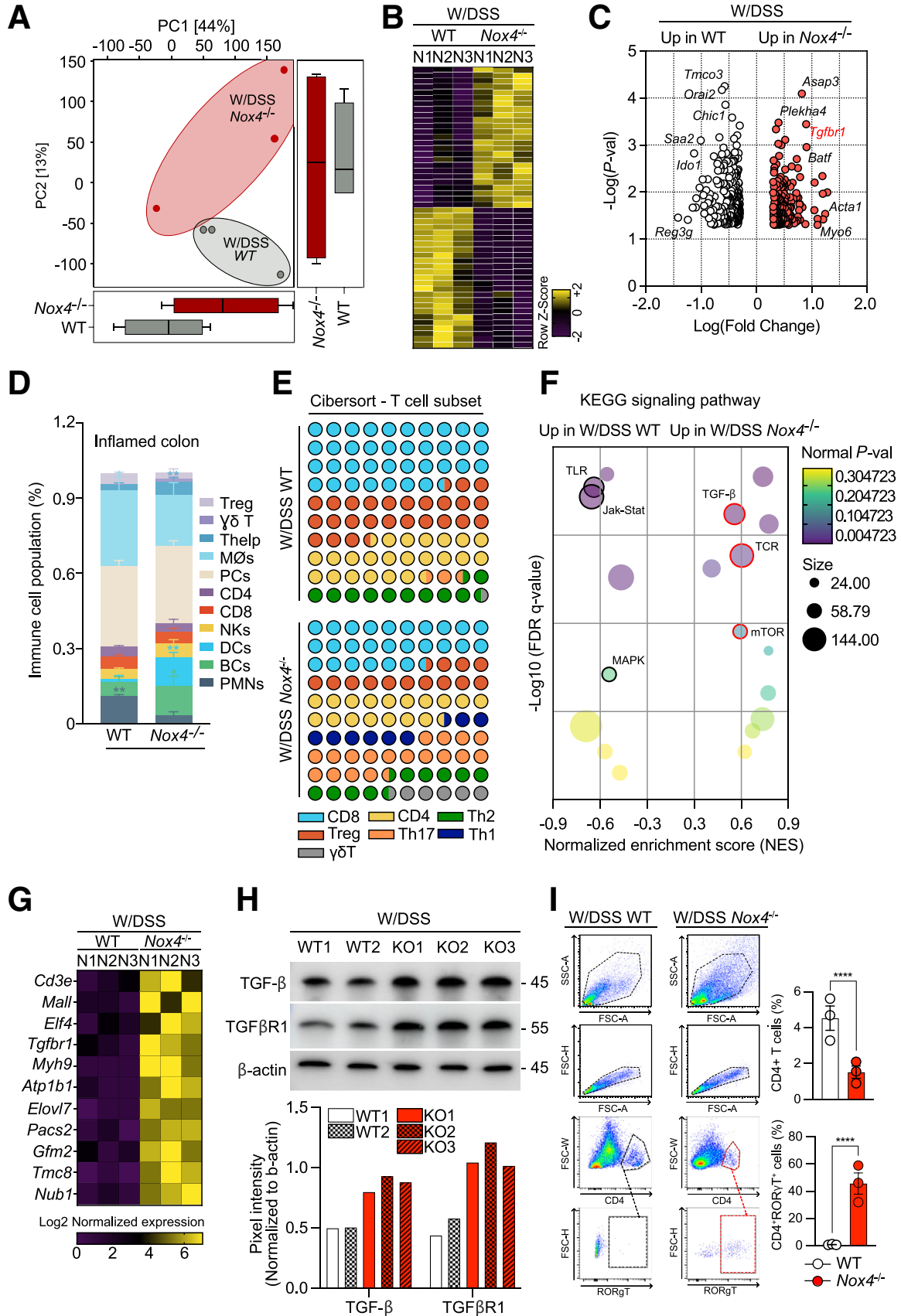


Figure 6. *Nox4* suppresses activation of canonical TGF- β signaling in vivo. (A) Scheme representing the canonical TGF- β signaling pathway. (B) Reverse-transcription quantitative PCR analysis of the expression of indicated TGF- β regulatory genes in the WT or *Nox4*^{-/-} mouse colon tissue; these mice differ from those used for RNA-seq ($n = 3$). *Black dots* represent untreated WT mice, and *red dots* represent untreated *Nox4*^{-/-} mice. (C) Active TGF- β level in WT (black) or *Nox4*^{-/-} (red) colon tissue lysates measured by enzyme-linked immunosorbent assay. (D) Immunoblotting of TGF- β and TGF β R1 protein levels in WT or *Nox4*^{-/-} colon tissue extracts; β -actin was used as an internal control. The band size was quantified by ImageJ. (E) Immunoblotting of pSmad2/3, Smad2/3, and Smad4 protein levels in cytosolic and nucleic fraction extracts from WT and *Nox4*^{-/-} colon tissues. Smad2/3 was used as the pSmad2/3 control proteins, and glyceraldehyde-3-phosphate dehydrogenase (GAPDH) and HDAC were used as the cytosol and nucleus control proteins, respectively. The band size was quantified by ImageJ. Representative immunofluorescence images of WT or *Nox4*^{-/-} colon sections stained with (F) TGF- β (red) and 4',6-diamidino-2-phenylindole (DAPI) (blue), or (G) TGF- β (green), CD11c (violet), and DAPI. Data are expressed as means \pm SD. ** $P < .01$, and **** $P < .001$ compared with WT. Cy, Cytosol; KO, Knock-out; LP, Lamina propria; Nu, Nucleus; P, pepsin-related.



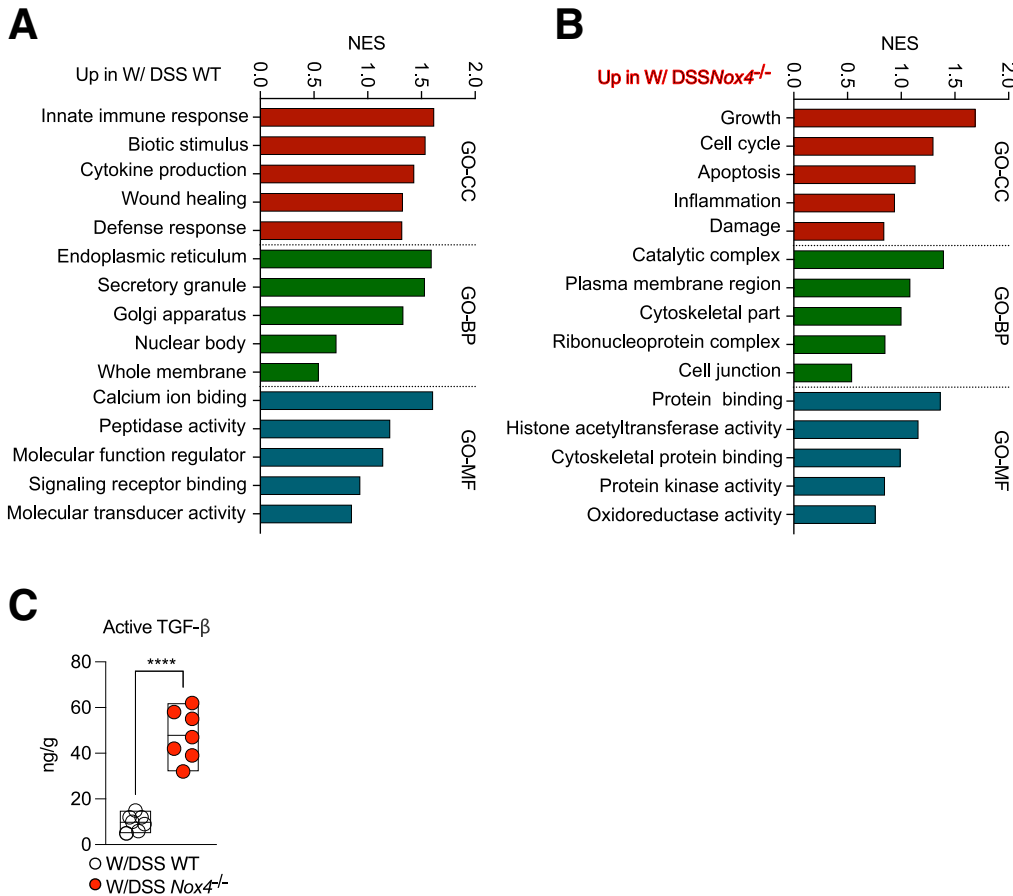


Figure 8. Related physiologic features in the WT and *Nox4*^{-/-} mouse colon. GO-term analysis of the up-regulated gene sets in (A) W/DSS WT DEGs and (B) W/DSS *Nox4*^{-/-} DEGs. (C) Active TGF- β levels in W/DSS WT or W/DSS *Nox4*^{-/-} colon tissue lysates determined by enzyme-linked immunosorbent assay. Data are expressed as means \pm SD. **** $P < .001$ compared with W/DSS WT.

kinase activity, histone acetyltransferase activity, and oxidoreductase activity (Figure 8B). KEGG pathway analysis indicated that the DEGs in W/DSS WT were enriched in the Toll-like receptor pathway, Janus kinase–signal transducer and activator of transcription pathway, and mitogen-activated protein kinase pathway, whereas DEGs in W/DSS *Nox4*^{-/-} were enriched in the TGF- β , T-cell receptor, and mammalian target of rapamycin pathways (Figure 7F). The heatmap confirmed that the expression levels of TGF- β target genes were increased significantly in DEGs of the W/

DSS *Nox4*^{-/-} group compared with those of the W/DSS group (Figure 7G).

These findings suggest that TGF- β signaling and its related fibrogenic and T-cell signals are increased consistently in the colons lacking *Nox4*, contributing to the maintenance of more severe inflammation. In line with these results from RNA-seq analyses, Western blot showed that TGF- β and TGF β R1 protein levels were increased in the W/DSS *Nox4*^{-/-} colon lysate compared with those of the W/DSS WT colon lysate (Figure 7H). ELISA confirmed that the

Figure 7. (See previous page). TGF- β signaling and its downstream molecules are up-regulated in DSS-induced colitis *Nox4*^{-/-} mice. (A) Local Fisher discriminant analysis plot for principal component analysis. Two-dimensional scores are readily distinguished between W/DSS WT (green) and W/DSS *Nox4*^{-/-} (red) samples. The shared areas indicate 95% CIs. (B) Total colonic cells sorted from W/DSS WT or W/DSS *Nox4*^{-/-} were subject to RNA-seq. The heatmap of RNA-seq data showing up-regulated (purple) and down-regulated (yellow) genes. (C) Volcano plot identifying significantly up-regulated genes in W/DSS WT (white) and W/DSS *Nox4*^{-/-} (red). CIBERSORT analysis of WT and *Nox4*^{-/-} colon tissues. The relative proportions of (D) 11 different immune cell types and (E) 7 T-cell lineage cell types are deconvoluted from the RNA-seq data using CIBERSORT. (F) Bubble plot showing significantly enriched KEGG pathways in the W/DSS WT and W/DSS *Nox4*^{-/-} DEGs. The bubble colors indicate P values, and the bubble size represents the expression level. (G) Heatmap of the expression of TGF- β -related genes from W/DSS *Nox4*^{-/-} DEGs. (H) Immunoblotting of TGF- β and TGF β R1 protein levels from W/DSS WT or W/DSS *Nox4*^{-/-} distal colon tissue extracts. β -actin was used as an internal control. The band size was quantified by ImageJ. (I) Flow cytometric plots showing the expression of ROR γ T on CD4⁺ T cells from W/DSS WT and W/DSS *Nox4*^{-/-} colon tissues. Data are expressed as means \pm SD. **** $P < .001$ compared with W/DSS WT. JAK-STAT, Janus kinase–signal transducer and activator of transcription pathway; MAPK, mitogen-activated protein kinase; mTOR, Mammalian target of rapamycin; NK, natural killer cell; p-val, P value; TCR, T cell receptor.

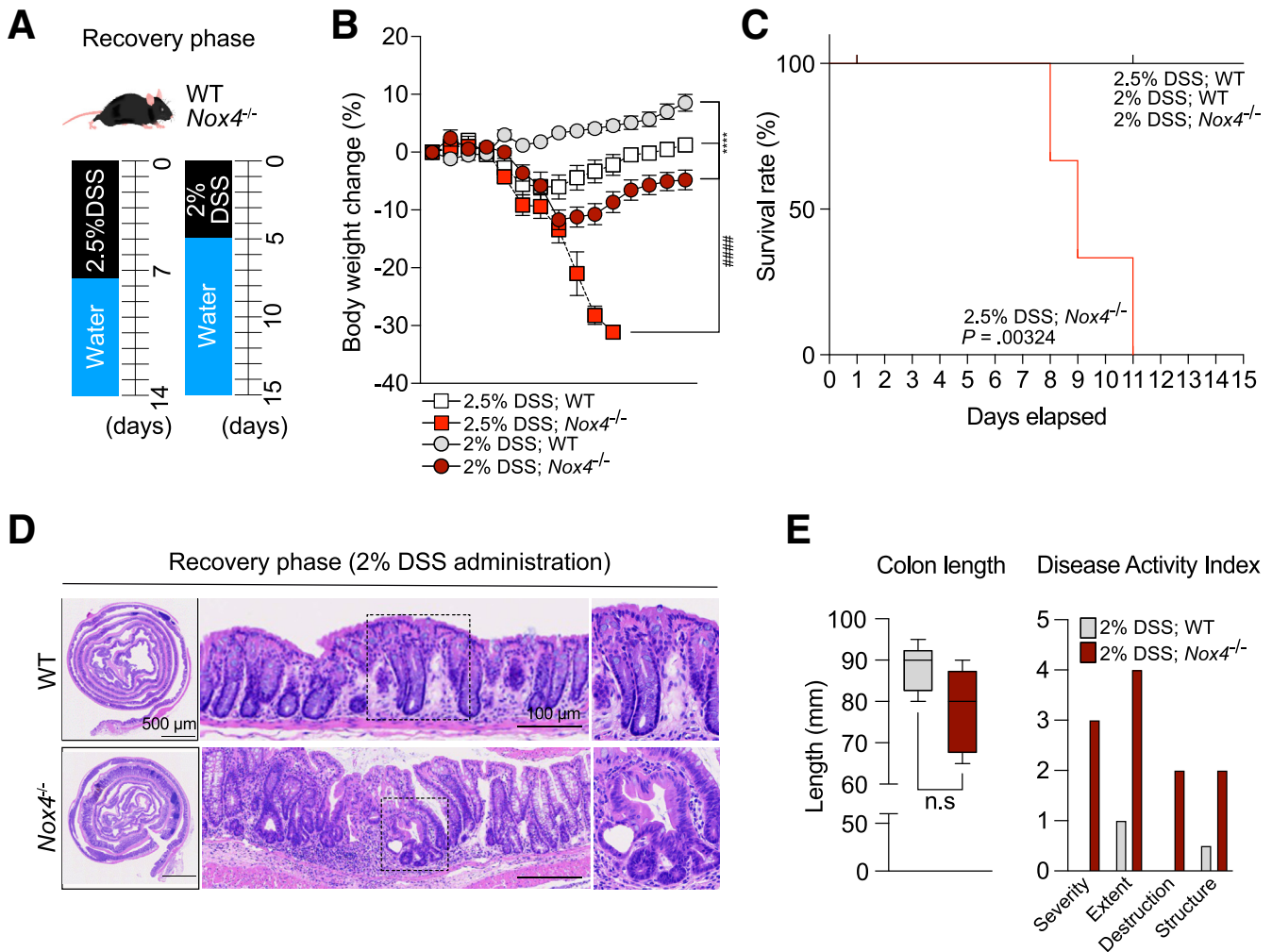


Figure 9. Loss of Nox4 disrupts tissue repair from DSS-induced colitis. (A) Experimental scheme for the recovery phase from DSS-induced murine colitis. (B) Body weight change for WT and Nox4^{-/-} mice with DSS-induced colitis and recovery phase measured daily (n = 5). (C) Survival probability of the recovery phase after DSS-induced colitis in WT and Nox4^{-/-} mice until day 15 (n = 5 per group). (D) Representative H&E staining images of colon tissues with the recovery phase after DSS-induced colitis in WT and Nox4^{-/-} mice. (E) Quantification of colon length and DAI score. DAI: severity, inflammatory severity (0–3); extent, inflammation extent (0, none; 1, mucosa; 2, submucosa; and 3, transmural), and epithelial change. Data are expressed as means ± SD. ****P < .001 compared with 2% DSS; WT vs. 2% DSS; Nox4^{-/-}; #####P < .001 compared with 2.5% DSS; WT vs. 2.5% DSS; Nox4^{-/-}.

active TGF-β level was increased by 2-fold in the W/DSS Nox4^{-/-} colon compared with the W/DSS WT colon (Figure 8C).

Flow cytometry analysis showed an increase in total CD4⁺ T cells in the W/DSS WT colon; however, approximately 59% of the CD4⁺ cells expressed RORγT⁺, a marker of Th17 cells, in the W/DSS Nox4^{-/-} colon, which was greater than that of the W/DSS WT colon (Figure 7I). Together, these findings confirmed an association of DSS-induced inflammation in the Nox4^{-/-} colon with Th17 cell lineage commitment.

Nox4 is Required for Intestinal Recovery After DSS-Induced Experimental Acute Colitis

Finally, we investigated whether Nox4 is required for recovery of intestinal inflammation (Figure 9A, left). Body

weight began to improve in W/DSS WT mice on day 9 (2 days after DSS treatment), whereas the body weight of W/DSS Nox4^{-/-} mice continuously reduced after 2.5% DSS administration and more rapid weight reduction was observed in the recovery phase. None of the W/DSS Nox4^{-/-} mice that experienced more than 30% weight loss survived (Figure 9B, 2.5% DSS; Nox4^{-/-} group); hence, the overall survival probability was diminished significantly in W/DSS Nox4^{-/-} mice (Figure 9C). We further performed experiments using 2% DSS administration to enter the recovery phase (Figure 9A, right). After 2% DSS administration, the 2% DSS; Nox4^{-/-} group showed a significant reduction in weight loss compared with the 2% DSS; WT group (Figure 9B), although there was no significant difference in survival rate (Figure 9C).

During the recovery phase, 2% DSS; WT mice displayed epithelial repair, mucosal healing, and only moderate

Table 1.Antibodies Used in This Study

Antibody	Dilution	Vendor	Catalog
NOX4	1:100	LsBio	LS-C313066
Cytochrome B245	1:1000	Bio-Rad	MCA4685
F4/80	1:500	Cell Signaling	70076
CD163	1:1000	Novus	NB110-59935
CD127	1:1000	eBioscience	14-1271-82
Ki-67	1:1000	Abcam	ab16667
TGF- β	1:100	Genetex	GTX21279
TGF β R1	1:100	R&D Systems	MAB5871
pSmad2/3	1:1000	Cell Signaling	8828
Smad2/3	1:1000	Cell Signaling	8685
Smad4	1:1000	Cell Signaling	46535
CD11c	1:300	Cell Signaling	97585
β -actin	1:5000	Abcam	ab8227
GAPDH	1:5000	Abcam	ab8245
HDAC1	1:1000	Abcam	ab280198
PE anti-mouse CD4	1:100	BioLegend	100408
Pacific blue anti-Foxp3	1:100	BioLegend	126409
Alexa 488 anti-ROR γ T	1:100	R&D Systems	IC9125G-025
Cy3 AffiniPure donkey anti-mouse	1:500	Jackson ImmunoResearch	715-165-151
Donkey anti-mouse IgG Alexa 488	1:500	Invitrogen	A-21202

GAPDH, glyceraldehyde-3-phosphate dehydrogenase; HDAC, Histone deacetylase; PE, Phycoerythrin.

inflammation on day 15. Conversely, the 2% DSS; *Nox4*^{-/-} mice still showed crypt atrophy, extended goblet cells, and severe immune cell infiltration (Figure 9D). In addition, colon length did not differ between the 2% DSS; *Nox4*^{-/-} group compared with the 2% DSS; WT group (Figure 9E, left), and the DAI showed that the 2% DSS; *Nox4*^{-/-} group had more severe symptoms than the WT group (Figure 9E, right).

Collectively, these results indicate that *Nox4* is crucial in the recovery process, and its absence can slow down the recovery rate.

Discussion

This study provides evidence that lack of *Nox4* leads to activation of TGF- β signaling in the normal colon, followed by a shift to a moderate fibrogenic phenotype and Treg recruitment as a type 2 immune response. Consequently, *Nox4*^{-/-} mice suffered from more intense mucosal damage, an increased immune response, and more severe fibrosis from DSS-induced colitis than WT mice, resulting in recovery failure leading to death.

Table 2.Primer Sequences Used in This Study

Genes	Sequence	Accession number
<i>TNF</i>	F: GGTGCCTATGTCTCAGCCTCTT R: GCCATAGAAGCTGATGAGAGGGAG	NM_013693
<i>I11b</i>	F: TGGACCTCCAGGATGAGGACA R: GTTCATCTCGGAGCCTGTAGTG	NM_008361
<i>Col1a1</i>	F: CCTCAGGGTATTGCTGGACAAC R: CAGAAGGACCTTGTTGCCAGG	NM_007742
<i>Col3a1</i>	F: GACCAAAAGGTGATGCTGGACAG R: CAAGACCTCGTGCTCCAGTTAG	NM_009930
<i>Tnc</i>	F: GAGACCTGACACGGAGTATGAG R: CTCCAAGGTGATGCTGTTGTCTG	NM_011607
<i>Tgfb1</i>	F: TGATACGCCTGAGTGGCTGTCT R: CACAAGAGCAGTGAGCGCTGAA	NM_011577
<i>Tgfb1</i>	F: TGCTCCAAACCACAGAGTAGGC R: CCCAGAACACTAAGCCCATTGC	NM_009370
<i>Tgfb2</i>	F: CCTACTCTGTCTGTGGATGACC R: GACATCCGTCTGCTTGAACGAC	NM_009371

F, forward; R, reverse.

Although a previous study reported that *Nox4* does not play a role in fibrosis in the murine colitis model, an increase in *Tgfb1* expression was detected with 2.5% DSS-induced colitis in *Nox4*^{-/-} mice.¹⁷ This result was observed after 6 days of administration of 2.5% DSS and 9 days after recovery with water for only 3 days. In our experiment, 2.5% DSS was administered for 14 days, which induced more severe damage in the colon. This is in line with a previous study showing differences in the severity of tissue damage depending on the DSS concentration and duration of administration in the establishment of the DSS-induced murine colitis model.⁴³

Although *Nox4* is considered to be closely related to tissue fibrosis, its specific role in fibrosis progression remains controversial. *Nox4*-induced ROS promotes cell apoptosis and mesenchymal cell differentiation and activation, leading to tissue fibrosis.^{18,19,30,44,45} *Nox4* was reported to play a critical role in the murine lung, leading to alveolar cell death and subsequent bleomycin-induced fibrosis by myofibroblast activation,^{18,30} and to attenuate Carbon tetrachloride (CCl₄)-induced liver injury, hepatocyte apoptosis, and liver fibrosis.⁴⁵ Conversely, another study showed that *Nox4* contributed to protecting against renal fibrosis in murine kidneys with chronic renal injury by inhibiting tubular cell apoptosis and oxidative stress.²⁰ Specifically, *Nox4* reduced *Hif1a* expression and antioxidant molecules in the Kelch-like ECH-associated protein 1 (Keap1) – Nuclear factor (erythroid-derived 2) (Nrf) pathway, thereby inhibiting ROS production, suggesting that *Nox4* may positively regulate antioxidant activity in the kidney.²⁰

Similarly, our results showed that loss of *Nox4* caused increased oxidation-reduction signaling with a consequent increase of ROS levels in the mouse colon tissue. The increase in ROS caused by deletion of *Nox4* in the murine colon is similar to the previously reported role of *Nox4* in the kidney, which inhibits ROS and regulates downstream signaling. These results correlated with the finding that *Nox4* suppressed ROS production in the colon and inhibited TGF- β signaling and its downstream fibrosis-related and type 2 immunity-related signals. Based on the functional enrichment analysis results of DEGs identified in the *Nox4*^{-/-} colon, collagen-associated signaling was up-regulated, consistent with changes in collagen protein level, and Treg cell lineage activation was up-regulated along with positive regulation of type 2 immunity. These data suggest that increased ROS stimulate the TGF- β -mediated immune response, such as type 2 immunity for host defense, and also activated immune suppression by Treg cells for immune tolerance.⁴⁶

The TGF- β signaling pathway is broadly associated with tissue physiology, including collagen synthesis⁴⁷ and Treg cell lineage commitment.⁴⁸ Moreover, the loss of *Nox4* altered the subsets of T cells stimulated by consistently activated TGF- β in the normal and inflammatory colons. TGF- β signaling can directly induce the differentiation of Foxp3⁺ Tregs and ROR γ T⁺ Th17 cells from naïve CD4⁺ T cells.^{49,50} Under normal conditions (ie, without DSS treatment), *Nox4*^{-/-} mice showed significantly increased infiltration of Foxp3⁺ Treg cells. Tregs are involved in immune

suppression, especially against commensal bacteria in the intestine. Infiltration of Foxp3⁺ Tregs along with increased ROS in the *Nox4*^{-/-} colon triggered TGF- β activation, proinflammatory cytokine (*Tnf* and *Il1 β*) expression, and F4/80⁺ macrophage infiltration. Therefore, the increase in Tregs is considered to be owing not only to TGF- β activation, but also represents a defense mechanism to regulate the inflammatory immune response in the *Nox4*^{-/-} mouse colon.

After induction of DSS-induced inflammation, the Treg population decreased and ROR γ T⁺ Th17 cells expanded. This result shows that *Nox4* regulates the Treg/Th17 balance during colitis; however, further studies are needed to determine the underlying mechanism. Recent studies have shown that Th17 cells are more abundant in patients with active IBD and play a causative role in IBD-associated colorectal cancer.^{51–53} Colorectal cancer typically shows a compact infiltrate of proinflammatory cytokine-producing cells. Among the tumor-infiltrating immune cells, T cells are switched into functional populations that secrete a large number of Th17-driven cytokines (interleukin [IL]17A, IL12, and IL22), tumor necrosis factor- α , and IL6. This population then promotes colon tumorigenesis and survival via signal transducer and activator of transcription 3/nuclear factor- κ B activation.⁵⁴ Although we did not identify the role of *Nox4* in colorectal cancer, Helfinger et al¹⁵ reported that *Nox4* can recognize DNA damage and suppress the oxidation of Protein kinase B (AKT), thereby playing a protective role in the DSS/Azoxymethane (AOM) murine colorectal cancer model. Although they did not describe the immune response of DSS/AOM-induced colorectal cancer in *Nox4*^{-/-} mice, our findings suggest that Th17 cells and related cytokines may enhance the survival and growth of colorectal cancer in *Nox4*^{-/-} mice.

Increased oxidative stress has long been implicated in the development of murine colitis. The NOX family has been suggested as a major contributor to intestinal inflammation progression.^{7,55} *Nox1* and *Duox2* are expressed in the intestinal epithelium and are the primary sources of ROS in the gastrointestinal tract; a deficit of these genes is related to increased disease severity of colitis. Recently, several studies have shown that deletion of *Nox4* induces more severe colitis^{16,17} and increases the risk of colorectal cancer.¹⁵ Conditional deletion of *Nox4* in fibroblasts and enterocytes was reported to lead to a higher tumor burden, especially from endothelial cells, and fibroblast-specific deletion of *Nox4* resulted in more rapidly developed tumors than the epithelial cell-specific deletion of *Nox4* mice. We found that *Nox4* is expressed in a nonepithelial cell population, suggesting that *Nox4* may determine the severity of colonic damage by regulating ROS-driven TGF- β signaling in the colonic epithelial cells.

In conclusion, we elucidated that genetic deletion of *Nox4* leads to the progression of more severe fibrotic colitis and subsequent recovery failure. Loss of *Nox4* increased oxidative stress in the colon tissues and subsequently activated canonical TGF- β signaling permanently. Furthermore, TGF- β -mediated T-cell lineage commitment (Treg and Th17 cells) and fibrosis-related signal influenced colitis

progression. Our findings on the role of *Nox4* in murine colitis highlight that regulation of the redox signal can be a valuable target for the successful treatment of patients with IBD.

Materials and Methods

Mice and Model Establishment

All animal experimental protocols were approved by the Institutional Animal Care and Use Committee (IACUC 2017-0258). Eight-week-old C57BL6/J male mice were used for in vivo experiments. Animals were housed in a specific pathogen-free facility under a 12-hour light-dark cycle and fed PicoLab Rodent Diet 20 (LabDiet, St. Louis, MO).

Nox4-null mice (*Nox4*^{-/-}) were established using clustered regularly interspaced short palindromic repeats and CRIPR-associated protein 9 (CRISPR/Cas9) technology with the deletion of exon 4 (Figure 1A). In addition, to test the influence of immune cells expressing *Nox* family members on fibrotic features in DSS colitis, we also generated *Nox2*-null (*Nox2*^{-/-}) mice (Figure 1B).

Previous studies have reported that *Nox4*^{-/-} mice are susceptible to damage by a DSS regimen.^{16,17} In this study, WT or *Nox4*^{-/-} 8-week-old male mice were administered 2.5% DSS (MP Biochemicals, Santa Ana, CA) in drinking water for 14 days to induce fibrotic colitis; fresh DSS solution was prepared every 2 days.²⁴ For the recovery phase, mice were administered 2% (w/v) DSS in the drinking water for 5 days, followed by a recovery period of 10 days with autoclaved tap water. Control mice received only autoclaved tap water. Daily weight changes and the DAI of mice were recorded.⁵⁶ DSS-induced colitis activity was scored according to body weight loss (0–4), stool frequency (0–3), and rectal bleeding (0–3).

Pathologic Analysis

Mice were killed and immediately perfused with ice-cold PBS in the left ventricle. The colon tissue was fixed with ice-cold 4% paraformaldehyde overnight at 4°C. The colon tissue was processed into a Swiss roll, then dehydrated, paraffin-embedded, and sectioned (5 μm). The sections were deparaffinized with xylene 3 times for 20 minutes each, absolute EtOH 3 times for 10 minutes each, 90% EtOH twice for 10 minutes each, and 75% EtOH for 10 minutes, and then stained with H&E. The sectioned tissue slides were dehydrated and mounted with a Shandon synthetic mount solution (Thermo Scientific).

Immunohistochemistry

During an inflammatory reaction in the colon, immune cell infiltration is characterized by an increase in proinflammatory cytokines in the colitis tissue.⁵⁷ To assess the immunologic phenotype in DSS-induced WT and *Nox4*^{-/-} mice, we performed immunohistochemistry of immune cell markers in the colon sections. Paraffin-embedded mouse colon sections were heated at 60°C for 1 hour and cooled to room temperature (22°C ~ 25°C). Deparaffinization and tissue rehydration were performed in xylene, graded

ethanol, and distilled water, as described earlier. Antigen retrieval was performed using Target Retrieval Solution (Dako) at high pressure for 15 minutes, and cooled down at 4°C for 1 hour. Sections were incubated with 3% H₂O₂ for 30 minutes to block endogenous peroxidase, followed by a reaction with Protein Block, Serum Free reagent (Dako) at room temperature for 2 hours. The sections were incubated with primary antibodies overnight at 4°C (Table 1). The sections were washed using PBS and incubated with Envision+ system horseradish peroxidase-labeled polymer anti-rabbit or mouse secondary antibody (Dako) at room temperature for 20 minutes. Slides were developed with a liquid 3,3'-diaminobenzidine tetra hydrochloride+ substrate chromogen system (Dako), counterstained with Mayer's hematoxylin (Dako) solution, dehydrated, and mounted. For immunofluorescence staining, primary antibody incubation was performed as described earlier, followed by incubation with cyanine-3 (Cy3)-labeled goat anti-mouse IgG (Jackson ImmunoResearch) or Alexa488-labeled donkey anti-rabbit IgG (Invitrogen) at room temperature for 1 hour. Slides were washed using PBS, counterstained with 4,6-diamino-2-phenylindole (Sigma), and mounted using Pro-Long Gold Antifade Reagent (Invitrogen).

TGF-β Activity

The level of active TGF-β was measured using a TGFβR1 kinase ELISA system according to the manufacturer's instructions (Promega, Madison, WI). To measure active TGFβR1, freshly isolated colon lysates were activated with 1 N HCl.

RNA-seq

Total RNA was isolated using TRIzol reagent (Invitrogen). RNA quality was assessed by an Agilent 2100 bioanalyzer using the RNA 6000 Nano Chip (Agilent Technologies, Amstelveen, The Netherlands), and RNA quantification was performed on an ND-2000 spectrophotometer (Thermo, Inc).

According to the manufacturer's instructions, library construction was performed for control and test RNAs using the QuantSeq 3' mRNA-Seq Library Prep Kit (Lexogen, Inc). In brief, each 500 ng total RNA sample was hybridized with an oligo-dT primer containing an Illumina-compatible sequence at its 5' end, and reverse-transcription was performed. After degradation of the RNA template, second-strand synthesis was initiated by a random primer containing an Illumina-compatible linker sequence at its 5' end. The double-stranded library was purified using magnetic beads to remove all reaction components. The library was amplified to add the complete adapter sequences required for cluster generation. The library was purified from PCR components. High-throughput sequencing was performed as single-end 75-bp sequencing using the NextSeq 500 platform (Illumina, Inc).

QuantSeq 3' mRNA-Seq reads were aligned using Bowtie2.⁵⁸ Bowtie2 indices were either generated from the genome assembly sequence or the representative transcript sequences for aligning to the genome and transcriptome. The

alignment file was used for assembling transcripts, estimating their abundances, and detecting DEGs between untreated WT (W/O WT) and *Nox4*^{-/-} (W/O *Nox4*^{-/-}) distal colon samples and W/DSS WT and W/DSS *Nox4*^{-/-} distal colon samples based on counts from unique and multiple alignments using coverage in bedtools.⁵⁹ The read count data were processed based on the quantile normalization method using the EdgeR package of R software (version 3.6.1) with Bioconductor (<http://www.bioconductor.org>).⁶⁰ The raw count data were first preprocessed using quality-control checks and lowly expressed genes were removed. We then normalized the data using the trimmed mean of M values method. We defined DEGs using linear models in DESeq2 v1.22.1 and applied significance criteria based on Benjamini–Hochberg false-discovery rate-adjusted *P* values less than .05.

Three-dimensional principal component analysis was performed using Python (version 3.6 or higher) (Python software foundation) with the following libraries installed: NumPy (for generating sample data) (Numpy community), Pandas (for loading the data set) (Pandas development team), Scikit-learn (for applying principal component analysis) (Scikit-learn community), and Matplotlib (for visualizing data) (Matplotlib development team). To explore the functional processes and pathways, we performed functional enrichment analysis for each module's eigengenes separately. We used the Database for Annotation, Visualization, and Integrated Discovery online tool version 6.8 to extract significant GO functional terms, including biological processes, molecular function, and cellular components, as well as KEGG pathways. The results of the KEGG pathway were visualized using Prism 9 (GraphPad software), and Enrichment Map (Enrichment map developers) was sorted based on enrichment score and false discovery rate values. To ensure the accuracy of the analysis, we performed gene set permutations 100 times. We selected significant items based on a *P* value threshold of less than .05. Gene set enrichment analysis for comparisons of 2 sample groups (*Nox4*^{-/-} vs WT) was performed in Gene set enrichment analysis v4.3.2 (Broad Institute, Cambridge, MA) using updated guidelines. To identify the cell types present and estimate their relative subsets, we used the CIBERSORT tool available at <http://cibersort.stanford.edu>. We used the RNA expression profiles of each sample to characterize the infiltration of 22 immune cell types and obtained an abundance ratio matrix of 15 immune cell types based on a significance threshold of *P* < .05.

Reverse-Transcription Quantitative PCR

Freshly isolated colon tissues were immersed in RNAlater stabilization solution (Invitrogen; Thermo Fisher Scientific, Inc) and incubated overnight at 4°C. Total RNA extraction was performed with TRIzol reagent (Invitrogen; Thermo Fisher Scientific) following the manufacturer's instructions. Contaminating genomic DNA was removed with Recombinant DNase1 (Takara Bio, Inc, Shiga, Japan), and the RNA was quantified using a Nanodrop spectrophotometer (Thermo Fisher Scientific). One milligram template RNA was reverse-transcribed using the ImProm-II reverse transcription System (Promega).

Western Blot

Freshly isolated colon tissues were immersed in RIPA solution (Sigma Aldrich). Colon lysates were loaded on 8%–15% polyacrylamide gels and transferred to polyvinylidene fluoride membranes (Millipore). Specific primary antibodies were used to detect the expression of proteins (Table 1). After incubation with horseradish peroxidase-conjugated secondary antibodies, membranes were developed using Signal West Femto Maximum Sensitivity Substrate (Thermo Scientific) with the LAS chemiluminescent imaging system (Amersham).

Flow Cytometry

To detect CD4⁺ and Foxp3⁺ Tregs or RORγT⁺ Th17 cells in the colon, single cells were isolated from the colon sections, as described previously.⁶¹ The cells were blocked with fragment crystallizable (Fc) Block (BD Biosciences) in fluorescence-activated cell sorter (FACS) buffer (0.5% fetal bovine serum, 10 mmol/L EDTA, and 0.05% NaN₃ in PBS) for 30 minutes at 4°C, followed by washing with FACS buffer. The cells were incubated with phycoerythrin-conjugated anti-mouse CD4 (BioLegend) and Pacific blue-conjugated anti-mouse Foxp3 (BioLegend) or Alexa 488-conjugated anti-mouse RORγT (R&D Systems) for 1 hour at 4°C. After washing with FACS buffer, the cells were sorted after gating for the live CD4⁺ and Foxp3⁺ cell fractions on a FACS Aria II cell sorter (BD Biosciences) for quantification.

Statistical Analysis

Data are presented as the means ± SD. Significant differences were evaluated by Student *t* test, Mann–Whitney *U* tests, or 1-way analysis of variance as appropriate using Prism9 (GraphPad Software). *P* < .05 was considered statistically significant.

References

1. Choi YY, Lee JK, Kim HS, et al. Medications and the risk of colorectal cancer in patients with inflammatory bowel diseases: use of the landmark method. *Yonsei Med J* 2021;62:997–1004.
2. Mak JWY, Ng SC. Epidemiology of fibrostenosing inflammatory bowel disease. *J Dig Dis* 2020;21:332–335.
3. Pircalabioru G, Aviello G, Kubica M, et al. Defensive mutualism rescues NADPH oxidase inactivation in gut infection. *Cell Host Microbe* 2016;19:651–663.
4. Ahrne S, Hagslatt ML. Effect of lactobacilli on paracellular permeability in the gut. *Nutrients* 2011; 3:104–117.
5. Roy S, Khanna S, Nallu K, et al. Dermal wound healing is subject to redox control. *Mol Ther* 2006;13:211–220.
6. Coant N, Ben Mkaddem S, Pedruzzi E, et al. NADPH oxidase 1 modulates WNT and NOTCH1 signaling to control the fate of proliferative progenitor cells in the colon. *Mol Cell Biol* 2010;30:2636–2650.
7. Kato M, Marumo M, Nakayama J, et al. The ROS-generating oxidase Nox1 is required for epithelial restitution following colitis. *Exp Anim* 2016;65:197–205.

8. Aviello G, Knaus UG. NADPH oxidases and ROS signaling in the gastrointestinal tract. *Mucosal Immunol* 2018;11:1011–1023.
9. Lee KA, Cho KC, Kim B, et al. Inflammation-modulated metabolic reprogramming is required for DUOX-dependent gut immunity in *Drosophila*. *Cell Host Microbe* 2018;23:338–352 e5.
10. Kim SH, Lee WJ. Role of DUOX in gut inflammation: lessons from *Drosophila* model of gut-microbiota interactions. *Front Cell Infect Microbiol* 2014;3:116.
11. Chen X, Jiang L, Han W, et al. Artificial neural network analysis-based immune-related signatures of primary non-response to infliximab in patients with ulcerative colitis. *Front Immunol* 2021;12:742080.
12. Sadler T, Bhasin JM, Xu Y, et al. Genome-wide analysis of DNA methylation and gene expression defines molecular characteristics of Crohn's disease-associated fibrosis. *Clin Epigenetics* 2016;8:30.
13. Pan LL, Ren Z, Liu Y, et al. A novel danshensu derivative ameliorates experimental colitis by modulating NADPH oxidase 4-dependent NLRP3 inflammasome activation. *J Cell Mol Med* 2020;24:12955–12969.
14. Dong S, Chen M, Dai F, et al. 5-Hydroxytryptamine (5-HT)-exacerbated DSS-induced colitis is associated with elevated NADPH oxidase expression in the colon. *J Cell Biochem* 2019;120:9230–9242.
15. Helfinger V, Freiherr von Gall F, Henke N, et al. Genetic deletion of Nox4 enhances cancerogen-induced formation of solid tumors. *Proc Natl Acad Sci U S A* 2021;118:e2020152118.
16. Han C, Sheng Y, Wang J, et al. NOX4 promotes mucosal barrier injury in inflammatory bowel disease by mediating macrophages M1 polarization through ROS. *Int Immunopharmacol* 2022;104:108361.
17. Stenke E, Aviello G, Singh A, et al. NADPH oxidase 4 is protective and not fibrogenic in intestinal inflammation. *Redox Biol* 2020;37:101752.
18. Hecker L, Vittal R, Jones T, et al. NADPH oxidase-4 mediates myofibroblast activation and fibrogenic responses to lung injury. *Nat Med* 2009;15:1077–1081.
19. Cheng Q, Li C, Yang CF, et al. Methyl ferulic acid attenuates liver fibrosis and hepatic stellate cell activation through the TGF-beta1/Smad and NOX4/ROS pathways. *Chem Biol Interact* 2019;299:131–139.
20. Nlandu Khodo S, Dizin E, Sossauer G, et al. NADPH-oxidase 4 protects against kidney fibrosis during chronic renal injury. *J Am Soc Nephrol* 2012;23:1967–1976.
21. Cucoranu I, Clempus R, Dikalova A, et al. NAD(P)H oxidase 4 mediates transforming growth factor-beta1-induced differentiation of cardiac fibroblasts into myofibroblasts. *Circ Res* 2005;97:900–907.
22. Jiang F, Liu GS, Dusting GJ, et al. NADPH oxidase-dependent redox signaling in TGF-beta-mediated fibrotic responses. *Redox Biol* 2014;2:267–272.
23. Sareila O, Kelkka T, Pizzolla A, et al. NOX2 complex-derived ROS as immune regulators. *Antioxid Redox Signal* 2011;15:2197–2208.
24. Bao S, Carr ED, Xu YH, et al. Gp91(phox) contributes to the development of experimental inflammatory bowel disease. *Immunol Cell Biol* 2011;89:853–860.
25. Vinay DS, Kwon BS. 4-1BB (CD137), an inducible costimulatory receptor, as a specific target for cancer therapy. *BMB Rep* 2014;47:122–129.
26. Adorno-Cruz V, Liu H. Regulation and functions of integrin alpha2 in cell adhesion and disease. *Genes Dis* 2019;6:16–24.
27. Ito TK, Ishii G, Chiba H, et al. The VEGF angiogenic switch of fibroblasts is regulated by MMP-7 from cancer cells. *Oncogene* 2007;26:7194–7203.
28. Susmi TF, Rahman A, Khan MMR, et al. Prognostic and clinicopathological insights of phosphodiesterase 9A gene as novel biomarker in human colorectal cancer. *BMC Cancer* 2021;21:577.
29. Seoane J, Gomis RR. TGF-beta family signaling in tumor suppression and cancer progression. *Cold Spring Harb Perspect Biol* 2017;9:a022277.
30. Carnesecchi S, Deffert C, Donati Y, et al. A key role for NOX4 in epithelial cell death during development of lung fibrosis. *Antioxid Redox Signal* 2011;15:607–619.
31. Hiraga R, Kato M, Miyagawa S, et al. Nox4-derived ROS signaling contributes to TGF-beta-induced epithelial-mesenchymal transition in pancreatic cancer cells. *Anticancer Res* 2013;33:4431–4438.
32. Park SH, Rhee J, Kim SK, et al. BATF regulates collagen-induced arthritis by regulating T helper cell differentiation. *Arthritis Res Ther* 2018;20:161.
33. Galbavy W, Lu Y, Kaczocho M, et al. Transcriptomic evidence of a para-inflammatory state in the middle aged lumbar spinal cord. *Immun Ageing* 2017;14:9.
34. Roma-Rodrigues C, Fernandes AR. Genetics of hypertrophic cardiomyopathy: advances and pitfalls in molecular diagnosis and therapy. *Appl Clin Genet* 2014;7:195–208.
35. Cheng C, Hua J, Tan J, et al. Identification of differentially expressed genes, associated functional terms pathways, and candidate diagnostic biomarkers in inflammatory bowel diseases by bioinformatics analysis. *Exp Ther Med* 2019;18:278–288.
36. Saeterstad S, Ostvik AE, Royset ES, et al. Profound gene expression changes in the epithelial monolayer of active ulcerative colitis and Crohn's disease. *PLoS One* 2022;17:e0265189.
37. Wang L, Oh WK, Zhu J. Disease-specific classification using deconvoluted whole blood gene expression. *Sci Rep* 2016;6:32976.
38. Grimes D, Johnson R, Pashos M, et al. ORAI1 and ORAI2 modulate murine neutrophil calcium signaling, cellular activation, and host defense. *Proc Natl Acad Sci U S A* 2020;117:24403–24414.
39. Ye Z, Bayron Poueymiroy D, Aguilera JJ, et al. Inflammation protein SAA2.2 spontaneously forms marginally stable amyloid fibrils at physiological temperature. *Biochemistry* 2011;50:9184–9191.
40. Eugene SP, Reddy VS, Trinath J. Endoplasmic reticulum stress and intestinal inflammation: a perilous union. *Front Immunol* 2020;11:543022.

41. Carroll IM, Maharshak N. Enteric bacterial proteases in inflammatory bowel disease- pathophysiology and clinical implications. *World J Gastroenterol* 2013;19:7531–7543.
42. Hu Y, Xiong LL, Zhang P, et al. Microarray expression profiles of genes in lung tissues of rats subjected to focal cerebral ischemia-induced lung injury following bone marrow-derived mesenchymal stem cell transplantation. *Int J Mol Med* 2017;39:57–70.
43. Kim JJ, Shajib MS, Manocha MM, et al. Investigating intestinal inflammation in DSS-induced model of IBD. *J Vis Exp* 2012;60:3678.
44. Li ZM, Xu SY, Feng YZ, et al. The role of NOX4 in pulmonary diseases. *J Cell Physiol* 2021;236:1628–1637.
45. Jiang JX, Chen X, Serizawa N, et al. Liver fibrosis and hepatocyte apoptosis are attenuated by GKT137831, a novel NOX4/NOX1 inhibitor in vivo. *Free Radic Biol Med* 2012;53:289–296.
46. Chapoval S, Dasgupta P, Dorsey NJ, et al. Regulation of the T helper cell type 2 (Th2)/T regulatory cell (Treg) balance by IL-4 and STAT6. *J Leukoc Biol* 2010; 87:1011–1018.
47. Yun SM, Kim SH, Kim EH. The molecular mechanism of transforming growth factor-beta signaling for intestinal fibrosis: a mini-review. *Front Pharmacol* 2019;10:162.
48. Zhang S, Gang X, Yang S, et al. The alterations in and the role of the Th17/Treg balance in metabolic diseases. *Front Immunol* 2021;12:678355.
49. Dominguez-Villar M, Hafler DA. Regulatory T cells in autoimmune disease. *Nat Immunol* 2018;19:665–673.
50. Veldhoen M, Hocking RJ, Atkins CJ, et al. TGFbeta in the context of an inflammatory cytokine milieu supports de novo differentiation of IL-17-producing T cells. *Immunity* 2006;24:179–189.
51. Amicarella F, Muraro MG, Hirt C, et al. Dual role of tumour-infiltrating T helper 17 cells in human colorectal cancer. *Gut* 2017;66:692–704.
52. Kempski J, Brockmann L, Gagliani N, et al. TH17 cell and epithelial cell crosstalk during inflammatory bowel disease and carcinogenesis. *Front Immunol* 2017; 8:1373.
53. Perez LG, Kempski J, McGee HM, et al. TGF-beta signaling in Th17 cells promotes IL-22 production and colitis-associated colon cancer. *Nat Commun* 2020; 11:2608.
54. De Simone V, Franze E, Ronchetti G, et al. Th17-type cytokines, IL-6 and TNF-alpha synergistically activate STAT3 and NF-kB to promote colorectal cancer cell growth. *Oncogene* 2015;34:3493–3503.
55. Burgueno JF, Fritsch J, Gonzalez EE, et al. Epithelial TLR4 signaling activates DUOX2 to induce microbiota-driven tumorigenesis. *Gastroenterology* 2021;160:797–808 e6.
56. Wirtz S, Popp V, Kindermann M, et al. Chemically induced mouse models of acute and chronic intestinal inflammation. *Nat Protoc* 2017;12:1295–1309.
57. Xue G, Hua L, Zhou N, et al. Characteristics of immune cell infiltration and associated diagnostic biomarkers in ulcerative colitis: results from bioinformatics analysis. *Bioengineered* 2021;12:252–265.
58. Langmead B, Salzberg SL. Fast gapped-read alignment with Bowtie 2. *Nat Methods* 2012;9:357–359.
59. Quinlan AR, Hall IM. BEDTools: a flexible suite of utilities for comparing genomic features. *Bioinformatics* 2010; 26:841–842.
60. Gentleman RC, Carey VJ, Bates DM, et al. Bioconductor: open software development for computational biology and bioinformatics. *Genome Biol* 2004;5:R80.
61. Graves CL, Harden SW, LaPato M, et al. A method for high purity intestinal epithelial cell culture from adult human and murine tissues for the investigation of innate immune function. *J Immunol Methods* 2014; 414:20–31.

Received December 28, 2022. Accepted May 9, 2023.

Correspondence

Address correspondence to: Ki Taek Nam, DVM, PhD, Severance Biomedical Science Institute, Yonsei University College of Medicine, 50-1 Yonsei-ro, Seodaemun-gu, Seoul 03722, Korea. e-mail: kitaek@yuhs.ac.

CRedit Authorship Contributions

Yura Lee (Investigation: Lead; Software: Lead; Validation: Lead; Visualization: Lead; Writing – original draft: Lead)
 Sung-Hee Kim, PhD (Conceptualization: Supporting; Data curation: Supporting; Funding acquisition: Supporting; Project administration: Supporting; Writing – original draft: Supporting)
 Haengdueng Jeong (Data curation: Supporting; Investigation: Supporting; Software: Supporting; Visualization: Supporting)
 Kwang H. Kim (Formal analysis: Supporting; Investigation: Supporting)
 Donghun Jeon (Formal analysis: Supporting; Methodology: Supporting; Software: Supporting)
 Yejin Cho (Formal analysis: Supporting; Methodology: Supporting; Visualization: Supporting)
 Daekee Lee (Methodology: Supporting; Resources: Lead)
 Ki Taek Nam, DVM, PhD (Conceptualization: Lead; Data curation: Lead; Funding acquisition: Lead; Resources: Lead; Supervision: Lead; Writing – original draft: Equal; Writing – review & editing: Lead)

Conflicts of interest

The authors disclose no conflicts.

Funding

This research was supported by the Brain Korea 21 Project for Medical Science at Yonsei University (K.T.N.), the Bio and Medical Technology Development Program of the National Research Foundation of Korea grant 2022R1A2C3007850 (K.T.N.), National Research Foundation of Korea grant 2022M3A9F3016364 (K.T.N.), the Korean Mouse Phenotyping Project grant 2016M3A9D5A01952416 (K.T.N.), and National Research Foundation of Korea grant 2020R111A1A01052033 (S.-H.K.).

Data Availability

The raw data have been submitted and can be accessed at the Korean Nucleotide Archive using accession number PRJKA230579.